Energy loss by non-relativistic electrons and positrons in liquid water

ARTICLE *in* NUCLEAR INSTRUMENTS AND METHODS IN PHYSICS RESEARCH SECTION B BEAM INTERACTIONS WITH MATERIALS AND ATOMS · SEPTEMBER 2002

Impact Factor: 1.12 · DOI: 10.1016/S0168-583X(02)00693-6

ELSEVIER

Nuclear Instruments and Methods in Physics Research B 194 (2002) 237–250

NIM B
Beam Interactions with Materials & Atoms

www.elsevier.com/locate/nimb

Energy loss by non-relativistic electrons and positrons in liquid water

Simon M. Pimblott [a,*], Laurens D.A. Siebbeles [b]

[a] *304C Notre Dame Radiation Laboratory, University of Notre Dame, Notre Dame, IN 46556-0579, USA*
[b] *Interfaculty Reactor Institute, Mekelweg 15, 2629 JB Delft, The Netherlands*

Received 18 September 2001; received in revised form 27 November 2001

Abstract

Inelastic collision cross-sections, mean free paths, stopping powers, energy loss distributions, mean energy losses and csda ranges are evaluated for non-relativistic electrons and positrons in liquid water using a formalism in which the response of the medium is expressed employing the experimental dipole oscillator strength distribution. Monte Carlo track structure simulations employing the calculated inelastic collision cross-sections, and elastic cross-sections evaluated using partial wave methods, are used to determine the energy dependence of positron and electron path-lengths, penetrations, and non-homogeneous energy deposition distributions. The calculated data are discussed, and compared and contrasted. The energy loss properties of electrons and positrons that depend only on the differential inelastic collision cross-section are similar for particle energies $\gtrsim 1$ keV, but there are apparent differences for lower energies. The energy loss properties depending on the size of the energy transfer events and on the differential inelastic collision cross-section differ for all particle energies. The differences found are the consequence of electron indistinguishability on the inelastic cross-section for the electron. Non-homogeneous energy deposition distributions of positrons with energy less than 1 keV are significantly more forward directed than those of electrons with the same initial energy. The differences are due to the larger inelastic collision cross-section of a positron compared to an electron, and its effect on the relative numbers of inelastic and elastic collisions.

Keywords: Positron; Liquid water; Implantation; Attenuation; Range

1. Introduction

With the development and the regular use of positron emission tomography (PET) in medicine [1] and of positrons to characterize the structure of materials in industry [2] it is necessary to understand the physical and chemical effects of positrons on matter. In addition, positron radiolysis is of fundamental importance in the elucidation of radiation damage in biological systems. The multiply damaged sites produced at a track-end in DNA are blamed for most of the lethal damage inflicted by radiation [3,4]. The annihilation rate of a positron depends on its local environment, so the chemistry of the thermalized positron (and its track) provides

* Corresponding author. Tel.: +1-219-631-7151; fax: +1-219-631-8068.
E-mail address: simon.m.pimblott.1@nd.edu (S.M. Pimblott).

0168-583X/02/$ - see front matter
PII: S0168-583X(02)00693-6

a time-resolved, observable probe of the track-end [5]. The positron has the same mass and the opposite charge of the electron, and the structure of a positron track is frequently assumed to be similar to that of an electron [5]. There must, however, be differences due to the consequences of electron indistinguishability on the energy loss properties. These differences may be significant in, for instance, determining the spatial resolution of PET images [6] where despite significant recent improvements in detector size, overall resolution of the image is limited. The resolution of PET images is determined by the understanding of a variety of non-technological factors, one of which is knowledge of the positron range (distribution).

To detail the effects of all types of ionizing radiation, it is important to understand the energy-loss processes of the radiation particles as they pass through the medium of concern. There have been a large number of Monte Carlo studies of the track structure of electrons in water (typical examples are described in references [7–10]), however, studies of positrons [11–13] and high-LET, heavy ions [14–16] are very limited [17]. One difficulty with performing these studies is the need for reliable, realistic cross-sections for the condensed phase [18]. Recently [19–23], a formalism describing energy loss by energetic electrons in condensed media has been developed which incorporates the effects of phase by using the appropriate dipole oscillator strength distribution of the medium. This treatment approximates the generalized dielectric response function of the medium by quadratically extending the dipole oscillator strength distribution into the energy-momentum plane using an approximation developed by Ashley [24]. This approximation allows a first-order extension of the Born approximation to include collisions with non-zero momentum transfer [19]. Experimentally based dipole oscillator strength distributions are available for a number of condensed systems including several different phases of water [25–29]. The validity of this approach for the evaluation of the inelastic energy loss properties of electrons and positrons has been addressed in some detail by comparing experimental data for the gas phase with the predictions of the theory [20,21,30]. The calculations reproduce experiment from about ~50 eV (depending on the medium) to close to relativistic energies. No additional approximations are introduced into the theory in the condensed phase.

In this study, the methodology developed for energetic electrons is used to describe the energy loss properties of positrons following the methodology outlined in [31] for liquid hydrocarbons and polymers. The expressions derived for positrons, and those previously developed for electrons, are now evaluated for liquid water. The inelastic collision cross-sections obtained are then used, along with appropriate elastic collision cross-sections, to simulate the track structure of non-relativistic positrons and electrons. These simulations are used to estimate the different components of the particle ranges and the non-homogeneous energy deposition distributions. The results for the two different low-LET particles are compared and contrasted.

2. Methodology

2.1. Energy loss properties of positrons and electrons

The complex dielectric response function, $\varepsilon(q,\gamma)$, describes the response of the homogeneous medium to an energy transfer γ and a momentum transfer q. The probability of an energy loss γ per unit distance traveled by a non-relativistic electron or positron with incident energy, $E = v^2/2$, is given by [19,24]

$$\tau(E,\gamma) = \int \mathrm{Im}[-1/\varepsilon(q,\gamma)]\frac{\mathrm{d}q}{q}, \tag{1}$$

where the reduced atomic units defined by Ashley [24] are employed for the charge, e, and the mass, m, of the electron (positron), and for $\hbar$, i.e. they are all set equal to 1 to simplify the mathematics. This probability is related to a density normalized differential collision cross-section by, $N\,\mathrm{d}\sigma = \tau(E,\gamma)\,\mathrm{d}\gamma$, where N is the number density of molecules in the medium. The integration of the probability τ over all possible energy losses gives the inverse mean free path,

$$\Lambda^{-1}(E) = \int \tau(E,\gamma)\,\mathrm{d}\gamma, \tag{2}$$

while the integration of the differential cross-section gives the inelastic collision cross-section,

$$\sigma(E) = \frac{1}{N}\int \tau(E,\gamma)\,\mathrm{d}\gamma \tag{3}$$

with $\sigma(E) = (N\Lambda(E))^{-1}$. The stopping power of the medium for the particle is the mean energy loss per unit path-length and is given by

$$S(E) = \int \gamma\tau(E,\gamma)\,\mathrm{d}\gamma, \tag{4}$$

and the csda range, which is a measure of the distance traveled by the particle, is obtained by integrating the inverse stopping power, $R = \int_0^E \mathrm{d}E'/S(E')$.

The energy loss function, $\mathrm{Im}[-1/\epsilon(q,\gamma)]$ is not available for most condensed media, however, there is a considerable amount of optical data, i.e. in the limit $q \sim 0$. Ashley has suggested the basic approximation [24],

$$\mathrm{Im}[-1/\varepsilon(q,\gamma)] = \int \frac{\gamma'}{\gamma}\mathrm{Im}\left[-\frac{1}{\varepsilon(0,\gamma')}\right]\delta\left(\gamma - \left(\gamma' + \frac{q^2}{2}\right)\right)\mathrm{d}\gamma', \tag{5}$$

where γ' can be interpreted as a "binding energy", [19] to extend the energy loss function from the optical limit through the energy-momentum plane.

To evaluate the inelastic collision cross-section, the mean free path and the stopping power, the kinematic constraints must be considered; Consider what happens when an electron or positron with incident energy $v^2/2$ undergoes a collision with a molecular electron. The incident particle departs with energy $v_1^2/2$, a quantity of energy $v_2^2/2$ is given to the molecular electron and a contribution γ' is made to the system, that is to the binding energy (and the recoil of the target molecule). Energy conservation requires that $v^2/2 = v_1^2/2 + v_2^2/2 + \gamma'$, while the energy loss is given by $\gamma = v^2/2 - v_1^2/2 > \gamma'$. As electrons are indistinguishable, it is assumed that $v_1^2/2 > v_2^2/2 > 0$ (or $\gamma' > 2\gamma - v^2/2$) for the energy donor and the acceptor electrons after the collision. This is not the case for a positron.

In addition, since $\gamma = \gamma' + q^2/2$ and $v_1 = (v^2 - 2\gamma)^{1/2}$, conservation of momentum gives the equivalent inequalities $v - v_1 < q < v + v_1$ and $-(v^2 - 2) + v(v^2 - 2\gamma)^{1/2} > \gamma' > 0 > -(v^2 - 2\gamma), -v(v^2 - 2\gamma)^{1/2}$, which reduce to $0 < \gamma' < -(v^2 - 2\gamma) + v(v^2 - 2\gamma)^{1/2} = \gamma'_{\max}$ for $0 < \gamma < v^2/4$, and to

$$\begin{aligned}\gamma_- &= 1/4v^2(1 + 2\gamma'/v^2 - v(1 - 4\gamma'/v^2)^{1/2}) \\ &< \gamma < 1/4v^2(1 + 2\gamma'/v^2 + v(1 - 4\gamma'/v^2)^{1/2}) \\ &= \gamma_+.\end{aligned}$$

The allowed regions of the $\gamma - \gamma'$ energy plane are shown in Fig. 1 for an electron and a positron, shaded as denoted in the key. There is significant reduction of the allowed region of the $\gamma - \gamma'$ energy plane for an energetic electron compared to an energetic positron because of the possibility of electron exchange [31,32].

A formulation for evaluating the non-relativistic energy loss parameters for an energetic electron has been discussed previously [21–23]. The energy loss parameters for a non-relativistic positron are more straightforward to evaluate than those of an electron as it is not necessary to introduce electron exchange. In addition, at non-relativistic energies ($\lesssim 0.1$ MeV) virtual annihilation and subsequent recreation of an electron-positron pair can be ignored.

Making use of the optical approximation of Ashley [24] and the appropriate energy and momentum transfer constraints derived above gives

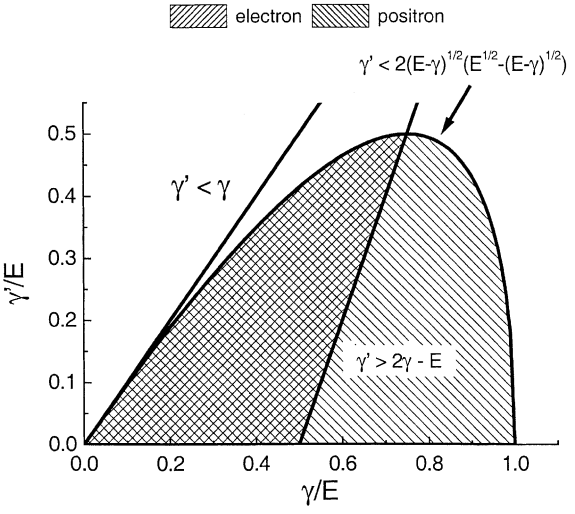

Fig. 1. The allowed region of the $\gamma - \gamma'$ plane for an electron and for a positron.

the following expression for the collision probability,

$$\tau(E,\gamma) = \frac{1}{2\pi E}\int_{\gamma_{\mathrm{low}'}}^{\gamma_{\mathrm{max}'}} \mathrm{Im}[-1/\varepsilon(0,\gamma)]G(\gamma,\gamma')\gamma'\,\mathrm{d}\gamma', \tag{6}$$

with $\gamma_{\mathrm{max}'}$ as defined above. For an electron

$$G_{\mathrm{elec}}(\gamma,\gamma') = \frac{1}{\gamma(\gamma-\gamma')} + \frac{1}{(v^2/2-\gamma)(v^2/2-\gamma+\gamma')} - \frac{1}{\sqrt{\gamma(\gamma-\gamma')(v^2/2-\gamma)(v^2/2-\gamma+\gamma')}} \tag{7}$$

with $\gamma_{\mathrm{low}'} = 0$ when $0 < \gamma < v^2/4$ or $\gamma_{\mathrm{low}'} = 2\gamma - v^2/2$ when $v^2/4 < \gamma < 3v^2/8$ [19], while for a positron

$$G_{\mathrm{pos}}(\gamma,\gamma') = \frac{1}{\gamma(\gamma-\gamma')} \tag{8}$$

and $\gamma_{\mathrm{low}'} = 0$ for all values of γ.

The expression for τ can now be used to evaluate the inverse mean free path (and the inelastic collision cross-section) and the stopping power. There are no singularities in the region of the $\gamma-\gamma'$ plane over which the integration is performed, so the order of integration can be reversed. The mathematical analysis gives

$$\Lambda^{-1}_{\mathrm{elec}}(E) = \frac{1}{2}\chi\int_0^{E/2}\mathrm{Im}[-1/\varepsilon(0,\gamma^{\gamma})] \times \left[\frac{1}{a}\ln\left[\frac{(1-a+s)(1+a-s)}{(1-a-s)(1+a+s)}\right] - \frac{2}{1+a}F(\arcsin(s/(1-a)),\frac{1-a}{1+a})\right]\frac{\gamma}{E}\mathrm{d}\gamma' \tag{9}$$

and

$$S_{\mathrm{elec}}(E) = \frac{1}{2}\chi\int_0^{E/2}\mathrm{Im}[-1/\varepsilon(0,\gamma')][\Sigma]\gamma'\,\mathrm{d}\gamma', \tag{10}$$

with

$$[\Sigma] = \ln\left[\frac{1-a}{1-a-s}\right] + \ln\left[\frac{(1+a)}{(1+a+s)}\right] + \frac{1}{a}\ln\left[\frac{(1-a+s)(1+a)}{(1-a)(1+a+s)}\right] - F\left(\arcsin(s/(1-a)),\frac{1-a}{1+a}\right) + \frac{1}{2}\ln\left(\frac{1}{a}(1+a/2-\sqrt{a(1+a/4)})\right)$$

for an electron [21] and

$$\Lambda^{-1}_{\mathrm{pos}}(E) = \frac{1}{2}\chi\int_0^{E/2}\mathrm{Im}[-1/\varepsilon(0,\gamma')] \times \ln\left[\frac{(1-a+s)(1+a-s)}{(1-a-s)(1+a+s)}\right]\mathrm{d}\gamma' \tag{11}$$

and

$$S_{\mathrm{pos}}(E) = \frac{1}{2}\chi\int_0^{E/2}\mathrm{Im}[-1/\varepsilon(0,\gamma')] \times \ln\left[\frac{1-a+s}{1-a-s}\right]\gamma'\,\mathrm{d}\gamma' \tag{12}$$

for a positron [31]. The variables a and s = are equal to γ'/E and $(1-2a)^{1/2}$, respectively. The function $F(x,y)$ is the incomplete elliptic integral of the first kind and the parameter χ is equal to $1/(\pi E)$ in the reduced units employed here. In the large E limit, the equations for the stopping power reduce to

$$S_{\mathrm{elec}}(E) = \chi\pi NZ(\ln(E^2/I) + 1 - \ln(2)) \tag{13}$$

and

$$S_{\mathrm{pos}}(E) = \chi\pi NZ(\ln(E^2/I) + 2\ln(2)), \tag{14}$$

where Z is the total number of electrons per water molecule and I is the mean excitation energy, which is defined by the sum rule, $Z\ln(I) = \int\gamma f(\gamma)\,\mathrm{d}\gamma$. These limiting expressions correspond to the non-relativistic versions of the Bethe (electron) and Bhabba (positron) stopping power formulae [33,34].

Track structure simulation studies, like those reported here, frequently make use the ratio of the cumulative inelastic cross-section, $\sigma(E,E')$, to the total inelastic cross-section, $\sigma(E,E_{\mathrm{max}'})$. This ratio,

commonly known as the Y function [35], describes the probability of an energy loss smaller than a value, E'. As mentioned earlier, the inelastic cross-section is $\sigma(E,E_{\max'})=(N\Lambda(E))^{-1}$. Since calculation of the cumulative inelastic cross-section involves an energy loss E' less than $E_{\max'}$ careful consideration of the bounds is necessary when performing the integration. For a positron the bounds are given by $0<\gamma'<-(v^2-2\gamma)+v(v^2-2\gamma)^{1/2}$ with the maximum possible value of $\gamma'(=E/2)$ occurring when $\gamma=3E/4$. This value of γ' does not correspond to the maximum energy loss possible, which is E. Consequently,

$$\begin{aligned}\sigma_{\rm pos}(E,E') &= \frac{1}{2}\frac{\chi}{N}\int_0^{\gamma_{\max'}} {\rm d}\gamma'\gamma'{\rm Im}[-1/\varepsilon(0,\gamma')]\\ &\quad\times\int_{\gamma_-}^{E'} {\rm d}\gamma G_{\rm pos}(\gamma,\gamma')\\ &= \frac{1}{2}\frac{\chi}{N}\int_0^{\gamma_{\max'}} {\rm d}\gamma'{\rm Im}[-1/\varepsilon(0,\gamma')]\\ &\quad\times\ln\left(\frac{(b-a)(1+a-s)}{b(1-a-s)}\right)\end{aligned}\tag{15}$$

for $0<E'<3E/4$, while for $3E/4<E'<E$,

$$\begin{aligned}\sigma_{\rm pos}(E,E') &= \frac{1}{2}\frac{\chi}{N}\int_0^{E/2} {\rm d}\gamma'\gamma'{\rm Im}[-1/\varepsilon(0,\gamma')]\\ &\quad\times\int_{\gamma_-}^{\gamma_+} {\rm d}\gamma G_{\rm pos}(\gamma,\gamma')\\ &\quad-\frac{1}{2}\frac{\chi}{N}\int_0^{\gamma'_{\max}} {\rm d}\gamma'\gamma'{\rm Im}[-1/\varepsilon(0,\gamma')]\\ &\quad\times\int_{E'}^{\gamma_+} {\rm d}\gamma G_{\rm pos}(\gamma,\gamma')\\ &= \Lambda_{\rm pos}^{-1}(E)/N\\ &\quad-\frac{1}{2}\frac{\chi}{N}\int_{\gamma_{\max'}}^{\gamma_+} {\rm d}\gamma'{\rm Im}[-1/\varepsilon(0,\gamma')]\\ &\quad\times\ln\left(\frac{b(1-a+s)}{(b-a)(1+a+s)}\right).\end{aligned}\tag{16}$$

Here $b=E'/E$, and a and s and the limits γ_-, γ_+ and $\gamma_{\max'}$ are as defined above.

The cumulative inelastic cross-section for an electron in a variety of different media has been discussed previously [19]. The bounds of the domain of integration are given by the inequalities $0<\gamma'<-(v^2-2\gamma)+v(v^2-2\gamma)^{1/2}$ and $\gamma'>2\gamma-v^2/2$. The maximum permissible energy loss is $3E/4$ when $\gamma'=E/2$. For an energy loss, E', in the range $0<E'<E/2$,

$$\sigma_{\rm elec}(E,E')=\frac{1}{2}\frac{\chi}{N}\int_0^{\gamma_{\max'}} {\rm d}\gamma'{\rm Im}[-1/\varepsilon(0,\gamma')][\Sigma_2]\gamma'/E,\tag{17}$$

with

$$\begin{aligned}[\Sigma_2] &= \frac{1}{a}\ln\left[\frac{(b-a)(1-b+a)(1+a-s)(1-a+s)}{b(1-b)(1-a-s)(1+a+s)}\right]\\ &\quad+\frac{2}{1+a}F\left(\arcsin\left(\frac{1+a-2b}{1-a}\right),\frac{1-a}{1+a}\right)\\ &\quad-\frac{2}{1+a}F\left(\arcsin(s/(1-a)),\frac{1-a}{1+a}\right),\end{aligned}$$

while for $E/2<E'<3E/4$,

$$\begin{aligned}\sigma_{\rm elec}(E,E') &= \Lambda_{\rm elec}^{-1}(E)/N-\frac{1}{2}\frac{\chi}{N}\\ &\quad\times\int_{\gamma'_{\max}}^{2E'-E} {\rm d}\gamma'{\rm Im}[-1/\varepsilon(0,\gamma')][\Sigma_3]\gamma'/E,\end{aligned}\tag{18}$$

with

$$\begin{aligned}[\Sigma_3] &= \frac{1}{a}\ln\left[\frac{(b-a)(1-b+a)}{b(1-b)}\right]\\ &\quad+\frac{2}{1+a}F\left(\arcsin\left(\frac{1+a-2b}{1-a}\right),\frac{1-a}{1+a}\right).\end{aligned}$$

These expressions are considerably more complicated than those for the positron, due to electron indistinguishability – the possibility of electron exchange and of its effect on the bounds.

3. Track structure simulation

The majority of simulation studies of the tracks of ionizing particles employ essentially the same technique [10,36–40], the trajectories of the primary particle and its daughter electrons are followed collision-to-collision until their energy is attenuated to a pre-defined cut-off. This type of simulation assumes that the medium is a continuum, and that

the distance between collisions can be obtained by sampling from a Poisson distribution with a mean free path, which is dependent on the energy of the particle. The nature of each collision is determined by the relative values of the cross-sections for the ionization, excitation, vibration and elastic processes at the appropriate particle energy. If the collision is inelastic, the energy loss is derived from the differential inelastic cross-section in energy via the Y function, discussed above. Trajectory deviations following inelastic events are evaluated from the kinematics, while those following elastic events are obtained by sampling from the differential elastic cross-section in angle obtain compiling experimental measurements of electron (positron) gas molecule scattering as detailed in Ref. [10]. In the following calculations, positron and electron trajectories are simulated to a final cut-off energy of 25 eV. The optical approximation, upon which the cross-section formalism is based, begins to break down at low energies. Comparison of experimental values with calculations for gas phase water show that the degree of uncertainty is small at 50 eV, but it is significant at <25 eV [20].

Despite the similarities between the various simulation methodologies in the literature, there are considerable differences between the cross-sections used to describe the physical processes occurring. LaVerne and Mozumder have studied the effect of phase on the energy loss properties of electrons [25]. They showed that it is not sufficient to use density-normalized inelastic cross-sections for gaseous water to represent liquid water. In the studies reported here, the inelastic collision cross-sections for positrons and for electrons are based on experimental dipole oscillator strength data for liquid water. In addition, the nature of the inelastic event is determined from the experimentally determined, energy-dependent photo-ionization efficiency of liquid water [41,42]. The total and the differential elastic cross-sections for positrons and for electrons are calculated using the algorithms of Salvat and co-workers, [43,44] which employ partial wave methods.

The energy dependences of the inelastic and elastic cross-sections for positrons and for electrons are shown in Fig. 2. At all energies, the inelastic cross-section for positrons is greater than

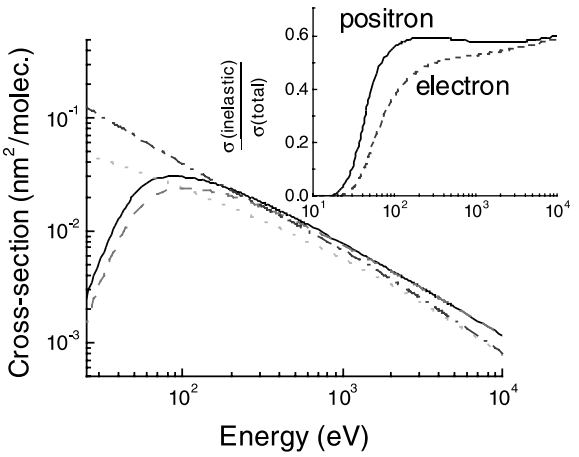

Fig. 2. Cross-sections for positrons and electrons in liquid water. Main figure: inelastic and elastic collision cross-sections. Positron: (—) inelastic; (· · · ·) elastic. Electron (– –) inelastic; (-·-·-) elastic. Inset: Probability of an inelastic collision, $\sigma(\text{inelastic})/\sigma(\text{total})$: (—) positron; (– –) electron.

that for electrons. The reverse is found for the elastic cross-section; the electron cross-section is greater than the positron cross-section. The differences between the two particles are significant at low energies (<1 keV), but negligible at 10 keV. These differences are clearly demonstrated in the inset of Fig. 2, which shows the inelastic contribution to the total cross-section. At 10 keV, the value of $\sigma(\text{inelastic})/\sigma(\text{total})$ is 0.60 for the positron and 0.59 for the electron; however, at lower energies the value for the positron is significantly larger than that for the electron.

4. Results and discussion

The central feature of the methodology developed for evaluating the energy-loss properties of electrons and positrons in matter is the role of the energy loss function $\text{Im}[-1/\epsilon(0,\gamma)]$ [45]. This is proportional to dipole oscillator strength distribution of the medium, $f(\gamma)$. Construction of the dipole oscillator strength distribution of liquid water from its optical properties was performed previously [22]. The dipole oscillator strength distribution has a broad peak with a maximum at $\sim$22 eV and a sharp rise at $\sim$534 eV corresponding

to the oxygen K-shell electrons [25]. The dipole oscillator strength distribution was checked using sum rules for the effective number of electrons that can receive an energy transfer, $Z_{\text{eff}} = \int f(\gamma)\,\mathrm{d}\gamma$ and for the mean excitation energy I_{eff}, which is defined by $Z_{\text{eff}} \ln(I_{\text{eff}}) = \int \gamma f(\gamma)\,\mathrm{d}\gamma$. In the high-energy limit, Z_{eff}, approaches the total number of electrons per water molecule, 10. The mean excitation energy is 74.9 eV, which compares favorably with the experimental value of 75 eV [46].

The differential Y function, $\mathrm{d}Y/\mathrm{d}\gamma$ [47] of a 1 keV electron and of a 1 keV positron are compared in Fig. 3. Physically, this distribution describes the probability of having an energy loss event in the range γ to $\gamma + \delta\gamma$, so it is effectively the differential energy loss distribution at the particle energy in question. As energetic electrons and positrons behave like "white light", their energy loss distributions resemble the dipole oscillator strength of liquid water [25]; however, there is a much larger density below ~50 eV in the differential energy loss distributions compared to the dipole oscillator strength distribution. This difference reflects the fact that there is a range of possible non-zero momentum transfers, which decreases with the energy of the particle. The effect of the oxygen K-shell on the differential energy loss distribution is not apparent for 1 keV electrons and positrons. Despite the sudden rise in the dipole oscillator strength distribution such energetic energy loss events are unlikely. For more energetic particles, there is a sharp rise in the density at this energy, though this rise is not as large as that in the dipole oscillator distribution. The most probable energy loss of a 1 keV electron and a 1 keV positron is ~23 eV, which corresponds to the peak of the dipole oscillator distribution. In fact, the most probable energy loss of an electron or positron is independent of the particle's energy.

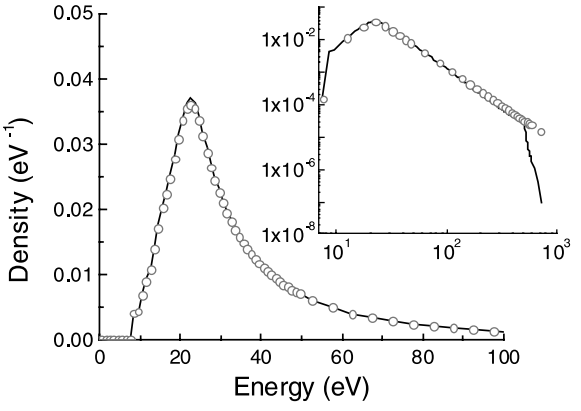

Fig. 3. Differential Y function of a 1 keV electron (—) and a 1 keV positron (○ ○ ○○) in liquid water.

For energy losses of magnitude 0–100 eV, the differential energy loss distribution of a 1 keV positron is similar to that for a 1 keV electron Fig. 3 shows that differences between the two distributions are small for energy losses smaller than 500 eV. At this energy, which corresponds to $\frac{1}{2}E$, the density drops precipitously for the electron, but not for the positron. The drop for the electron is due to the effect of electron exchange on its inelastic collision cross-section. The maximum energy loss of an electron is $\frac{3}{4}E$, but the probability of events greater than $\frac{1}{2}E$ is small. Energy losses of up to E are possible for the positron. Since by definition, the differential energy loss distribution is normalized to one, the differences observed at high energy imply differences at lower energy. The relative difference between the distributions for electrons and positrons of energy 1 keV, is sizable at energies >500 eV, however, the absolute magnitude of the density is small. As a result, the differences at low energies are hardly observable. This is not true for positrons and electrons of lower energy. If the differential energy loss distributions for electrons and positrons of energy 200 eV are compared, significant discrepancies are found over the complete range of possible energy losses.

The significance of the differences between the differential energy loss distributions is best demonstrated by comparing the mean energy loss for a particular incident particle energy. The mean energy loss of an electron or a positron is given by $\langle E' \rangle = \int \gamma(\mathrm{d}Y/\mathrm{d}\gamma)\mathrm{d}\gamma$. For a 1 keV electron it is 46.1 eV and for a 1 keV positron it is 52.2 eV. The dependence of the mean energy loss on the energy of the particle is listed in Table 1. Even though the most probable energy loss is independent of the particle's energy, the mean energy loss increases with the particle's energy. Larger energy losses

Table 1
Effect of particle energy on the mean energy loss of an electron and a positron

Particle energy (keV)	Mean energy loss (eV)		Percent difference
	Electron	Positron	
0.07	27.4	30.2	10.0
0.10	30.7	34.9	13.7
0.30	39.4	45.8	16.4
1.0	46.1	52.2	13.2
3.0	52.1	58.7	12.7
10.0	57.5	63.1	9.6
30.0	60.9	66.0	8.6
100.0	3.7	68.0	6.7

Table 2
Effect of particle energy on the density normalized mean free path of an electron and a positron in liquid water

Particle energy (keV)	Mean free path (μg/cm^2)	
	Electron	Positron
0.03	0.93	0.58
0.05	0.21	0.14
0.07	0.14	0.10
0.10	0.13	0.10
0.30	0.18	0.16
1.00	0.40	0.39
3.00	0.95	0.94
10.0	2.57	2.56
30.0	6.30	6.28
100.0	15.3	15.3

become possible as the particle energy increases. The positron has a larger mean energy loss than the electron for all particle energies. For an electron, the mean energy loss approximately doubles from ~30 eV at 100 eV to ~ 65 eV at 100 keV, while for a positron it grows from 35 eV to 68 eV over this energy range. The difference between the two particles decreases from ~14% at low energies to 10% at 10 keV and to 7% at 100 keV. The origins of the difference between electrons and positrons lies in the energy weighting of the differential Y function in the integral defining the mean energy loss. This weighting magnifies the differences, due to exchange, between the Y functions for positrons and electrons. These differences become less significant as the energy of the particles increases because the contribution of energy transfers greater than $\frac{1}{2}E$ to the Y function decreases.

The dependence of the density-normalized mean free path, $\rho\Lambda$, in liquid water of an electron and of a positron on the particle's energy is given in Table 2. (The density of the material, ρ is the number density, N, divided by Avogadro's constant, L_A, i.e. $\rho = N/L_A$.) For particle energy >1 keV, there is essentially no difference between the value for a positron and that for an electron. However, at lower energy, the positron has a significantly smaller mean free path than the electron; for 100 eV particles, the mean free path of an electron is ~25% larger than that of a positron. The discrepancy at low energy and the close correspondence at high energy are due to the effect of electron exchange on the inelastic collision cross-section. The mean free path is inversely proportional to the differential inelastic collision cross-section ($d\sigma$) and so depends on the probability τ. As a result, electron indistinguishability has a large effect at low particle energy (less than ~1 keV), but has little effect at higher particle energy.

The density normalized stopping power of liquid water for electrons and positrons is considered in Fig. 4. The energy dependence for positrons is very similar to that for electrons; there is a maximum at ~120–150 eV and a decrease with an $\sim E^{-3/4}$ dependence at high energy. However, there are considerable differences (>20%) between the absolute values of the density normalized

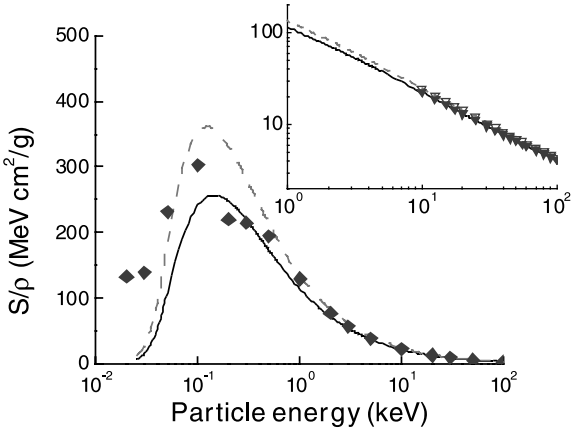

Fig. 4. Energy dependence of the density normalized stopping power, S/ρ, of non-relativistic electrons and positrons in liquid water. Electrons: (—) $S_{elec}(E)$, (◆) ICRU 16 [48], (▼) [46]; Positrons: (––) $S_{pos}(E)$, (▽) [46].

stopping powers for the two particles at low energies (<1 keV), and noticeable differences (~10%) at high energy. The maximum value of the density normalized stopping power, S/ρ of water for electrons is 258 MeV g/cm^2 and occurs at ~145 eV, while it is 361 MeV g/cm^2 at ~125 eV for positrons: this discrepancy is ~40%. The stopping power is the first energy moment of the probability τ, and so depends on the differential inelastic collision cross-section weighted by energy. This "energy weighting" leads to a larger stopping power for positrons than electrons, because of the increased probability of larger energy loss events. Also shown in Fig. 4 are the recommendations of ICRU 16 for the stopping power of liquid water for electrons, and the predictions of the stopping power of liquid water for energetic electrons and positrons made by Berger and Seltzer [46,48]. The stopping powers obtained using the formalism described here are in excellent agreement with these data (and other values available in the literature). The conventional Moeller and Bhahba theories for the stopping power of electrons and positrons, respectively, apply to energetic particles [33,34]. In the non-relativistic, high-energy limit, there is exact agreement with the formalism presented here. However, there are deviations at energies $\lesssim$ 200 eV.

Most experimental studies measure track-averaged quantities. The distribution of energy losses for the complete slowing down of 10 and 100 keV incident particles, including the attenuation of the daughter secondary electrons, to less than 5 keV (the conventional definition of a track-end in radiation chemistry) is shown in Fig. 5 for both electrons and positrons. The most probable energy loss is ~22 eV, irrespective of the particle type or energy. In contrast, the mean energy loss (including the final short-track track-end) does depend on the particle energy and type. At 10 keV, the mean energy loss for an electron track is ~97 eV compared to 103 eV for a positron track. The difference between the two values decreases as the incident energy increases, and there is no difference between the mean energy loss of high-energy electrons and high-energy positrons. At 100 keV, the mean energy loss for both types of incident particle is ~61 eV.

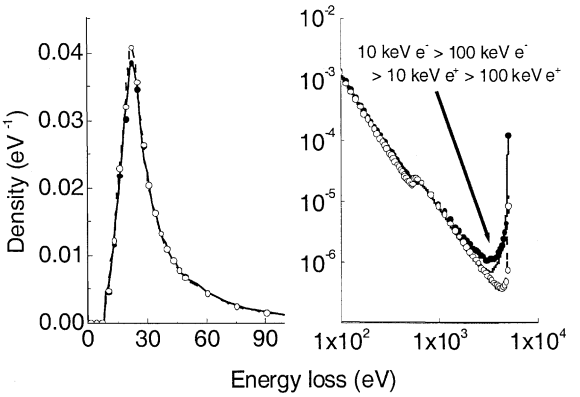

Fig. 5. Energy loss distributions for 10 and 100 keV incident electrons and positrons in liquid water. The distributions represent the attenuation of the incident particle and secondary daughter electrons to the short-track limit, 5 keV. Electrons: (—) 10 keV, (– –) 100 keV; positrons: (●) 10 keV, (○) 100 keV.

The incident energy dependences of the density normalized (csda) range, ρR, of an electron and of a positron in liquid water are given in Table 3. The density normalized csda range for a positron is smaller than that of an electron for energy less than ~1 keV, but essentially the same for energies $\gtrsim$ 2 keV. As the density normalized csda range is obtained by integrating the inverse stopping power, it effectively depends on the differential inelastic collision cross-section like the mean free path. Consequently, electron indistinguishability significantly increases the range of low-energy electrons compared to positrons, but results in little difference for higher energy particles. The csda ranges calculated for the electron are in good agreement with the recommendations of ICRU 16 for energies >2 keV, however, there are some discrepancies at lower energies. The ICRU recommendations are based upon semi-empirical range energy relationships with parameters inferred from the stopping power of the medium. The 'experimental' recommendations of the ICRU 16[48] for the stopping power of low energy electrons in liquid water were derived from measurements in air and collodion. These experiments are the only ones to use low energy electrons and they are often presented as representative of liquid water. However, calculations have shown that the stopping power of electrons below ~100 eV in

Table 3
Effect of initial energy on the pathlength of an electron and of a positron in liquid water

Particle energy (keV)	csda range (μg/cm^2)		Pathlength[a] (μg/cm^2)		Penetration[b] (μg/cm^2)	
	Electron	Positron	Electron	Positron	Electron	Positron
0.07	1.05	0.60	0.98	0.47	0.31	0.29
0.10	1.19	0.69	1.08	0.53	0.35	0.33
0.30	2.01	1.32	1.97	1.18	0.73	0.75
1.00	6.68	5.19	6.88	5.36	3.64	3.71
3.00	34.1	29.0	35.4	30.8	21.3	21.2
10.0	258	230	268	245	173	168
30.0	1770	1660	1817	1696	1190	1158
100.0	1.42×10^4	1.32×10^4	1.47×10^4	1.37×10^4	9.96×10^3	9.54×10^3

[a] Pathlength is the length of the trajectory the particle takes in traveling from its initial position, $\boldsymbol{X}_i$ and to its final position, $\boldsymbol{X}_f$.
[b] Penetration is the separation between $\boldsymbol{X}_i$ and $\boldsymbol{X}_f$ of the particle $= |\boldsymbol{X}_f - \boldsymbol{X}_i|$.

solid hydrocarbons and in gases are substantially greater than in liquid water [23,49].

Thus far the energy loss properties of electrons and of positrons in liquid water has been discussed using data calculated from deterministic relationships. The attenuation and the trajectory of an energetic radiation particle are stochastic in nature, and so the energy loss properties are amenable to simulation. Such studies have the advantage that more detailed information is obtained. Four different measures of the distance traveled by an energetic particle are available from the track structure simulations: (i) the path-length, (ii) the distance between the initial position ($\boldsymbol{X}_i$) and final position ($\boldsymbol{X}_f$), (iii) the axial component of the vector $\boldsymbol{X}_f - \boldsymbol{X}_i$ (i.e. parallel to the initial electron trajectory) and (iv) the absolute value of the radial component of the vector $\boldsymbol{X}_f - \boldsymbol{X}_i$ (i.e. perpendicular to the initial electron trajectory). The particle energy dependences of the path-length and the distance$|\boldsymbol{X}_f - \boldsymbol{X}_i|$ are included in Table 3. The path-length is the distance traveled by the radiation particles as it undergoes energy loss and its energy is attenuated, while the distance, $|\boldsymbol{X}_f - \boldsymbol{X}_i|$, corresponds to the actual penetration of the particle. The pathlength has a similar value and energy dependence to the csda range. Since the inelastic cross-section of a non-relativistic positron is greater than that of an electron of the same incident energy, the path-length of a positron is always smaller than that of an electron. For both positrons and electrons, there is a significant difference (about a factor of 2 at high energies) between the magnitudes of the path-length and the penetration distance; the trajectory of even an energetic particle is not a straight line.

The penetration of positrons is slightly larger than that of electrons for incident energies >300 eV, but it is smaller for energies lower than 300 eV. The differences between the values for the two types of particle reflect differences in the track structure. The change, from the penetration for positrons being greater than that for electrons to it being smaller, is due to the energy dependences of the inelastic and of the elastic cross-sections shown in Fig. 2. At high particle energies, the inelastic and elastic cross-sections of positrons and electrons are the same. At an energy of several keV, the elastic scattering cross-section for positrons becomes smaller than that for electrons, while the inelastic cross-sections of positrons and electrons begin to diverge at much lower energies, $\sim$300 eV. Thus, a positron of several keV undergoes fewer elastic scattering events than an electron of the same energy; this results in a greater penetration and less straggling. At low energies, the larger inelastic cross-section of the positron compared to the electron results in a shorter path-length and penetration even though the electron undergoes more elastic scattering events. The axial and radial components of the vector $\boldsymbol{X}_f - \boldsymbol{X}_i$ are compared in Table 4. For electrons, the mean values of the axial and radial components are similar in magnitude, while for positrons the axial component is always slightly larger than the radial component. This data supports the discussion above: the positron

Table 4
Effect of initial energy on the penetration of an electron and of a positron in liquid water

Particle energy (keV)	Axial penetration (μg/cm^2)		Radial penetration (μg/cm^2)	
	Electron	Positron	Electron	Positron
0.07	0.18	0.19	0.23	0.18
0.10	0.20	0.22	0.26	0.21
0.30	0.48	0.55	0.47	0.43
1.00	2.53	2.79	2.23	2.08
3.00	15.0	15.6	13.1	12.4
10.0	123	123	105	98.9
30.0	852	841	723	672
100.0	7264	7072	5896	5532

has few elastic scattering events and therefore a more forward directed trajectory.

Collision-by-collision simulation method provides a full three dimensional description of radiation particles track structure. The simulated profiles for the axial penetration and radial penetration of 1 keV positrons and electrons in liquid water are shown in Fig. 6. There are some substantive differences between the simulated profiles for positrons and those for electrons. Ten percent of the electrons are backscattered from the starting point compared to 5% of the positrons. The axial profile for electrons has less depth than that for positrons, and the radial profile is broader-the median of the radial penetration distribution for the electron is 10% larger than that of the radial penetration distribution for the positron. Positron implantation is frequently described using empirical Markovian penetration profiles with the form

$$P(z) = \frac{mz^{m-1}}{z_0^m} \exp(-(z/z_0)^m), \tag{19}$$

where m is the shape parameter and z_0 is the penetration parameter [50,51]. The value of the shape parameter determines the degree to which the profile is an exponential ($m = 1$) or a Gaussian ($m = 2$). The radial distribution is then assumed to have a Gaussian distribution with a standard deviation of $z_0/\sqrt{2}$ [50,51]. Also included in Fig. 7 is the best fit to the axial penetration profile of the equation for $P(z)$, which was obtained with $m = 1.91$ and $z_0 = 30.9$ nm. There are substantial

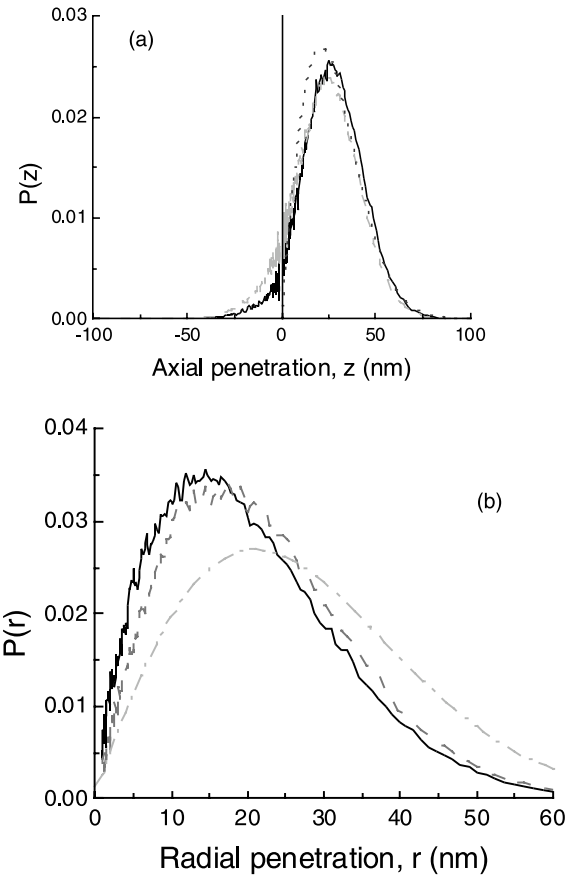

Fig. 6. Simulated profiles for the axial penetration (a) and radial penetration (b) of 1 keV positrons and electrons in liquid water. (—) positron, (– –) electron, (· · · ·) best fit to the axial penetration profile, $P(z)$, obtained with $m = 1.91$ and $z_0 = 30.9$ nm, (–·–·) inferred Gaussian radial distribution with a standard deviation of $z_0/\sqrt{2}$.

differences between the profiles obtained by simulation and those inferred assuming an empirical Markov penetration: the simulated penetration profile is deeper than the empirical profile, while the simulated radial profile is significantly narrower than the inferred Gaussian radial profile. A number of crude track structure simulation studies of positrons in atomic materials, specifically metals like aluminum, copper, silver and gold have been made with the goal of understanding positron implantation profiles [50,52–54]. These studies also found that the empirical Markovian treatment was unacceptable. The depth parameter obtained here for liquid water (~2.0) is similar, but higher than

the values obtained for silver (1.8) and gold (1.9) in Ref. [52] and for gold (1.7) in Ref. [54]. The fraction of backscattered positrons is independent of energy ($5.1 \pm 0.5\%$) for positrons of energy 1–30 keV. The fraction of backscattered positrons with an initial energy of 5 keV is 5.5%. This value is slightly smaller than the value, 8%, inferred from Fig. 5 of Ref. [50], which documents the variation of backscattered fraction with atomic number.

The energy dependences of the percentage backscatter, of m and of the ratio of the penetration parameter to the mean axial penetration, $z_0\langle z\rangle$, obtained by simulation for liquid water are shown in Fig. 7. The amount of positrons backscattered decreases as the initial energy increases. The shape parameter has no dependence on positron energy varying within between 1.9 and 2.2 over the energy range 1–30 keV, but increases at higher energies. The ratio $z_0/\langle z\rangle$ is independent of initial positron energy, therefore, as the mean axial penetration is a strong function of positron energy, the depth parameter is strongly dependent on positron energy. The effect of positron energy on the positron implantation profile in metals is reviewed in [50] and the parameter z_0 is shown to be dependent both on the material and on the positron energy.

The range of an energetic particle provides an estimate of the overall volume of the water involved in the radiolysis processes, but the rate of energy loss along the particle path varies greatly. To understand the non-homogeneous processes, which lead to the physical, chemical and biological consequences of radiolysis, a picture of the spatial distribution of the energy deposition is required. This information cannot be obtained from range data alone. A contour plot of the energy deposition density, D, in units of eV nm^{-3} for 1 keV positrons and electrons in liquid water is shown in Fig. 8. For both types of particle, the energy deposition density is peaked along the axis of the direction of the initial particle trajectory, with the maximum density located close to the initial position of the particle. This peak represents the first inelastic collision. The non-homogeneous dose dissipates as the distance from this point increases. The "pear-like" to "apple-like" change in the

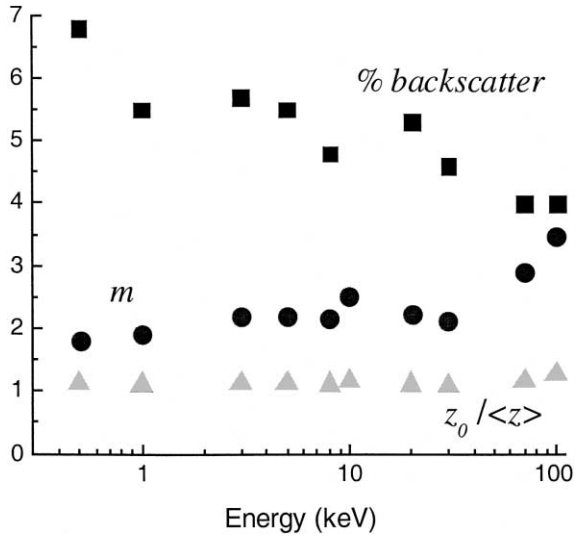

Fig. 7. Energy dependence of the percentage backscattered positrons (■), of the Markovian shape parameter m(●) and of the ratio of the penetration parameter to the mean axial penetration, $z_0\langle z\rangle$, (▲) for liquid water.

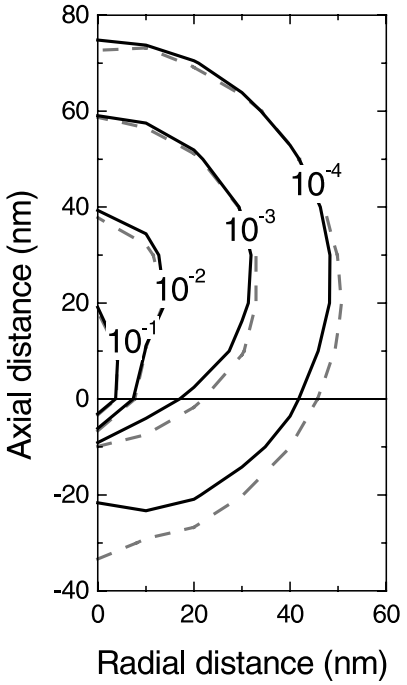

Fig. 8. Energy deposition density, D, in units of (eV nm^{-3}) for 1 keV positrons and electrons in liquid water. (—) positrons; (– –) electrons.

shape of the contors of the distributions reflects the increasing effects of the deviations in the trajectory due to inelastic and elastic collisions, and the changes in the rate of energy loss as the particle slows down. For electrons, there is significantly more back-scattered energy deposition than for positrons. This backscatter is largely due to the increased number of elastic collisions. When the elastic collisions are ignored, and σ (elastic) is arbitrarily set to zero, the backward scattered component of the density disappears. The apparently monotonic decrease in dose with radial distance is associated with the larger volume elements of the outer shells in the cylindrical coordinate system about the track axis.

A contour plot of the radial dose distributions, $2\pi rD$, in units of eV nm^{-2} of 1 keV positrons and electrons in liquid water is given in Fig. 9. For both positrons and electrons, the greatest radial dose is not in the axial direction, $r = 0$, but approximately in the direction of the vector $z = r$. Again the increased contribution of back-scattered energy deposition for the electron over the positron is apparent.

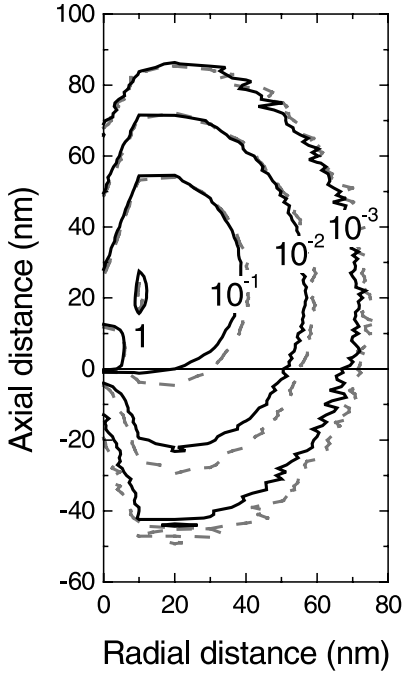

Fig. 9. Radial dose distribution, $2\pi rD$, in units of (eV nm^{-2}) for 1 keV positrons and electrons in liquid water. (—) positrons; (––) electrons.

5. Conclusions

Energy loss properties for non-relativistic electrons and positrons in liquid water are calculated using a formalism that is based on the quadratic extension of the dipole oscillator strength distribution into the energy-momentum transfer domain. At low ionizing radiation particle energies, there are significant differences between the energy loss properties of positrons and of electrons. These differences reflect the importance of electron exchange on the inelastic collision cross-section for electrons. At higher particle energies, the properties that depend on the zeroth energy moment of the differential inelastic collision cross-section, such as mean free path and csda range, are found to be very similar for the two particles. These properties are determined by the multitude of small energy loss events, which are of similar frequency for electrons and positrons. In contrast, energy loss properties that depend on the first energy moment of the differential inelastic collision cross-section, such as stopping power and mean energy loss, are different for the two particles. In this case, the infrequent, large energy loss events that are allowed for a positron, but not for an electron, are significant. The absence of these large energy loss events for electrons are due to the effects of electron exchange, which causes the maximum possible energy transfer for an electron to be smaller than for a positron.

Acknowledgements

The research described was supported in part by the Office of Basic Energy Science of the US Department of Energy. This is contribution NDRL-4333 of the Notre Dame Radiation Laboratory.

References

[1] J.M.M. Anderson, B.A. Mair, M. Rao, J. Control, Cybernetics 25 (1996) 1089.

[2] H. Yang, Y.C. Jean, Positron Annihilation, Trans Tech Publications, Brandrain, Switzerland, 1997, p. 40.
[3] D.T. Goodhead, H.P. Leenhouts, H.G. Paretzke, M. Terrissol, H. Nikjoo, R. Blaauboer, Radiat. Prot. Dosim. 52 (1994) 217.
[4] J.F. Ward, Radiat. Res. 86 (1981) 185.
[5] O.E. Mogensen, Positron Annihilation in Chemistry, Springer Verlag, Berlin, 1995.
[6] C.S. Levin, E.J. Hoffman, Phys. Med. Biol. 44 (1999) 781.
[7] H.G. Paretzke, J.E. Turner, R.N. Hamm, H.A. Wright, R.H. Ritchie, J. Chem. Phys. 84 (1986) 3182.
[8] D.T. Goodhead, H. Nikjoo, Int. J. Radiat. Biol. 55 (1989) 513.
[9] M.A. Hill, F.A. Smith, Radiat. Phys. Chem. 43 (1994) 265.
[10] S.M. Pimblott, J.A. LaVerne, A. Mozumder, J. Phys. Chem. 100 (1996) 8595.
[11] H. Iida, I. Kanno, S. Miura, M. Murakami, K. Takahashi, K. Uemura, IEEE Trans. Nucl. Sci. 33 (1986) 597.
[12] R.R. Raylman, B.E. Hammer, N.L. Christensen, IEEE Trans. Nucl. Sci. 43 (1996) 2406.
[13] D.W. Rickey, R. Gordon, W. Huda, Automedica 14 (1991) 355.
[14] D.J. Brenner, M. Zaider, Radiat. Prot. Dosim. 13 (1985) 127.
[15] V. Cobut, Y. Frongillo, J.P. Patau, T. Goulet, M.-J. Fraser, J.-P. Jay-Gerin, Radiat. Phys. Chem. 51 (1998) 229.
[16] Y. Frongillo, T. Goulet, M.-J. Fraser, V. Cobut, J.P. Patau, J.-P. Jay-Gerin, Radiat. Phys. Chem. 51 (1998) 245.
[17] A number of standard packages for calculating the physical effects of high energy electrons and positrons exist such as GEANT (available from the CERN Program Library), ITS (NERSC High Performance Computing Facility) and EGS. These simulation tools are not appropriate for investigating the collision-by-collision track structure of low and intermediate energy (< about 100 keV) radiation particles. Statistical fluctuations at low electron energies are better represented using a collision-by-collision simulation technique rather than an average stopping power or csda range based method.
[18] S.M. Pimblott, N.J.B. Green, in: R.G. Compton, G. Hancock (Eds.), Research in Chemical Kinetics, Elsevier, Amsterdam, 1995, p. 117–74.
[19] N.J.B. Green, J.A. LaVerne, A. Mozumder, Radiat. Phys. Chem. 32 (1988) 99.
[20] S.M. Pimblott, J.A. LaVerne, A. Mozumder, N.J.B. Green, J. Phys. Chem. 94 (1990) 488.
[21] S.M. Pimblott, J.A. LaVerne, J. Phys. Chem. 95 (1991) 3907.
[22] J.A. LaVerne, S.M. Pimblott, J. Phys. Chem. 99 (1995) 10540.
[23] J.A. LaVerne, S.M. Pimblott, Radiat. Res. 141 (1995) 208.
[24] J.C. Ashley, J. Electron, Spectrosc. Relat. Phenom. 46 (1988) 199.
[25] J.A. LaVerne, A. Mozumder, J. Phys. Chem. 90 (1986) 3242.
[26] G.D. Zeiss, W.J. Meath, J.C.F. MacDonald, D.J. Dawson, Radiat. Res. 63 (1975) 64.
[27] J.M. Heller, R.N. Hamm, R.D. Birkhoff, L.R. Painter, J. Chem. Phys. 60 (1974) 3483.
[28] M. Seki, K. Kobayashi, J. Nakahara, J. Phys. Soc. Jpn 50 (1981) 2643.
[29] K. Kobayashi, J. Phys. Chem. 87 (1983) 4317.
[30] J.A. LaVerne, S.M. Pimblott, A. Mozumder, Radiat. Phys. Chem. 38 (1991) 75.
[31] S.M. Pimblott, J.A. LaVerne, A.A. Garcia, L.D.A. Siebbeles, J. Phys. Chem. B. 104 (2000) 9607.
[32] J.C. Ashley, J. Appl. Phys. 69 (1991) 674.
[33] R.R. Roy, R.D. Reed, Interaction of photons and leptons with matter, Academic Press, New York, 1968.
[34] J.M. Jauch, F. Rohrlich, The theory of photons and electrons, Springer Verlag, New York, 1976.
[35] A. Mozumder, J.L. Magee, J. Chem. Phys. 45 (1966) 3332.
[36] M. Zaider, D.J. Brenner, W.E. Wilson, Radiat. Res. 95 (1983) 231.
[37] D.J. Brenner, M. Zaider, Radiat. Res. 98 (1984) 14.
[38] H.G. Paretzke, in: G.R. Freeman (Ed.), Kinetics of Nonhomogeneous Processes. A Practical Introduction for Chemists, Biologists, Physicists, and Materials Scientists, Wiley-Interscience, New York, 1987.
[39] J.E. Turner, R.N. Hamm, H.A. Wright, R.H. Ritchie, J.L. Magee, A. Chatterjee, W.E. Bolch, Radiat. Phys. Chem. 32 (1988) 503.
[40] L.D.A. Siebbeles, W.M. Bartzcak, M. Terrissol, A. Hummel, J. Phys. Chem. A 101 (1997) 1616.
[41] D.N. Nikogosyan, A.A. Oraesky, V.I. Rupasov, Chem. Phys. 77 (1983) 131.
[42] D.M. Bartels, R.A. Crowell, J. Phys. Chem. A 104 (2000) 3349.
[43] J.M. Fernandez-Varea, D. Liljequist, S. Csillag, R. Raty, F. Salvat, Nucl. Instr. and Meth. B 108 (1996) 35.
[44] F. Salvat, Radiat. Phys. Chem. 53 (1998) 247.
[45] J. Berkowitz, Photoabsorption, Photoionization and Photoelectron Spectroscopy, Academic Press, New York, 1979.
[46] M.J. Berger, S.M. Seltzer, Stopping Powers and Ranges of Electrons and Positrons, NBS, Washington DC, 1982.
[47] The differential energy loss distribution is directly proportional to the differential inelastic collision cross-section.
[48] ICRU Report 16. Linear Energy Transfer, ICRU Publications, Washington, DC, 1970.
[49] J.A. LaVerne, L. Wojnarovits, J. Phys. Chem. 99 (1995) 9862.
[50] V.J. Ghosh, K.G. Lynn, D.O. Welch, P. Int. Sch. Phys. 125 (1995) 683.
[51] G.R. Brandes, K.F. Canter, A.P. Mills, Phys. Rev. B 43 (1991) 10103.
[52] A. Aydin, Radiat. Phys. Chem. 59 (2000) 277.
[53] K.A. Ritley, K.G. Lynn, V.J. Ghosh, D.O. Welch, M. McKeown, J. Appl. Phys. 74 (1993) 3479.
[54] J.A. Baker, N.B. Chilton, K.O. Jensen, A.B. Walker, P.G. Coleman, Appl. Phys. Lett. 59 (1991) 2962.